



Hydrological drought dynamics and its teleconnections with large-scale climate indices in the Xijiang River basin, South China

Qingxia Lin^{1,2} · Zhiyong Wu³ · Jingjing Liu⁴ · Vijay P. Singh⁵ · Zheng Zuo²

Received: 27 January 2022 / Accepted: 20 July 2022 / Published online: 4 August 2022
© The Author(s), under exclusive licence to Springer-Verlag GmbH Austria, part of Springer Nature 2022

Abstract

Hydrological drought is a highly complex and extreme natural disaster, which has increased in deficit, areal extent, and frequency with the penetration of climate change impact. For better anticipating hydrological droughts, it is crucial to evaluate hydrological drought and its teleconnections with large-scale climate indices (LSCI) effectively. This study estimated the dynamics and patterns of hydrological drought in the near-real river networks by virtue of the standardized runoff index (SRI) based on VIC and large-scale routing model in the Xijiang River basin, and revealed their teleconnections with the climate indices. Results show that model simulation can reasonably reveal the hydrological drought evolutions in near-real river networks and effectively expose the drought downward spread along main channels. The drought spread distances in Hongshuihe and Yujiang Rivers are farther under the comprehensive influence of climate, topography, and watershed shape. Hydrological drought evolutions in the upper reaches are mainly manifested as three patterns, including S12 (simultaneous significant changes in drought intensity, concentration degree, and frequency), S7 (simultaneous significant changes in drought intensity and frequency), and S1 (single significant change in drought intensity). These drought dynamic patterns are majority affected by climate variation patterns M1 (warm and cold AMO), M3 (cold PDO), and M7 (warm AMO/AO). For decision-makers, this work is beneficial for understanding and anticipating hydrological droughts in the river networks, and further selecting management strategies for water resources.

Highlights

- The quantitative results of model simulation are reliable for drought evaluation.
- Drought concentration period delays and drought risk increases significantly.
- Dynamic evolutions of drought mainly manifest as three combinations patterns.
- Upstream drought is mainly affected by AMO, PDO, and AMO/AO.

Keywords Hydrological drought · Standardized runoff index · Hydrological modeling · Large-scale climate indices · Xijiang River basin

✉ Zhiyong Wu
wzyhhu@gmail.com

- ¹ Engineering Research Center of Eco-Environment in Three Gorges Reservoir Region, Ministry of Education, China
Three Gorges University, Yichang 443002, China
- ² College of Hydraulic and Environmental Engineering, Three Gorges University, Yichang 443002, China
- ³ College of Hydrology and Water Resources, Hohai University, Nanjing 210098, China
- ⁴ North China Electric Power Design and Research Institute, Beijing 100011, China
- ⁵ Department of Biological and Agricultural Engineering, Texas A&M University, College Station, TX 77843-2117, USA

1 Introduction

Drought is considered to be one of the most frequent, serious, and widely distributed natural disasters in the world (Mahmoudi et al. 2019; Monjo et al. 2020; Dikshit et al. 2021; Zhang et al. 2021). American Meteorological Society (AMS) has divided drought into four categories based on its specific area of impact: meteorological, agricultural, hydrological, and socioeconomic drought (Li et al. 2021; Kambombe et al. 2021). Lack of precipitation causes a meteorological drought but results in a hydrological drought as it propagates into more extensive areas along with the drainage network (Huang et al. 2017; Gu et al. 2020; Ding et al.

2021). Therefore, severe hydrological drought directly correlates with variability and availability of water resources and would affect agricultural production, urban water supply, ecological balance, and socioeconomic development (Chen et al. 2019).

Assessing the spatial–temporal dynamics of hydrological drought, not only helps to gain knowledge about its variabilities, but also improves the drought monitoring ability, thereby reducing its adverse impact (Diaz et al. 2019; Noorisameleh et al. 2021). Nowadays, the severity and distribution of hydrological drought have frequently been investigated on the database of river-gauging stations (Altn et al. 2020; Aghelpour et al. 2021; Katipolu et al. 2021), and the spatial distribution of hydrological drought is obtained by interpolation. However, the gauge-based drought monitoring accuracy is often limited by the sparse and uneven distribution of gauges, which is difficult to realistically reflect the non-uniformity characteristics of hydrological drought.

Compared with station-based monitoring, the hydrological modeling considers the land use, vegetation, and soil conditions of the underlying surface to obtain the runoff series of grid or sub-basin, so it can investigate the hydrological drought with higher spatial–temporal resolution (Zhang et al. 2018; Melsen and Guse 2019; Xing et al. 2020). Some researchers have used hydrological models, such as TOPography-based hydrological model (TOPMODEL), Hydrologiska Fyrans Vattenbalans model (HBV), Soil and Water Assessment Tool (SWAT), and Variable Infiltration Capacity model (VIC) to conduct hydrological drought researches and demonstrate model-based drought monitoring is effective (Zhu et al. 2019; Wu et al. 2019a; Veetil and Mishra 2020; Venegas-Cordero et al. 2021). Above diverse models have their own advantages in the mechanism of runoff generation. However, the subsequent calculations of runoff routing seem to have similar shortcomings, for overgeneralizing the routing routes and ignoring the regulation ability of grid or sub-basin, which may affect runoff accuracy in drought index construction.

In order to improve the calculation accuracy of the runoff routing, Lu et al. (2015) proposed a large-scale distributed routing model. The model firstly refers to the river network division method proposed by Yamazaki et al. (2009) to generate the near-real river network based on grid and sub-basin merged units. Then, take the merged unit as the grid representative area and calculate the response function of each unit based on the kinematic wave. Eventually, the diffusion wave is used to conduct the runoff routing between merged units (Wu et al. 2021). Compared with the traditional routing models, the improved model has a more reasonable structure, realistic river network, and higher precision. Therefore, it seems to be more beneficial for investigating the distributed characteristics of hydrological drought.

The distributed characteristics of hydrological drought are highly irregular in spatial and temporal dimensions. Sufficient evidence from previous studies has demonstrated that these variabilities are closely linked with climate indices such as the El Niño Southern Oscillation (ENSO), the Pacific Decadal Oscillation (PDO), the Atlantic Multidecadal Oscillation (AMO), and the Atlantic Oscillation (AO) (Talaee et al. 2014; Huang et al. 2016; Vazifekhah and Kahya 2019; Wu et al. 2019b; Abdelkader and Yerdelen 2022). For instance, Abdelkader and Yerdelen (2022) assessed the possible teleconnections between hydrological drought series and climate indices. They revealed a significant correlation between drought periods and ENSO, NAO, and AMO intense phases in Meriç Basin, Turkey. Vazifekhah and Kahya (2019) investigated the teleconnections of NAO, AO, PDO, SCAND, POLEUR, and EA/WR over 3-month hydrological drought indices in Konya Closed basin through cross-wavelet transform (XWT) technique, and showed significant relationship existed between climate and drought indices in some periods. Although the association between large-scale climate factors and hydrological drought has been confirmed, however, the spatially distribution characteristics of teleconnection are still unclear with the limitation of gauge-based drought monitoring.

The Xijiang River in southern China is known as the “golden waterway” with its important artery for China to construct the Pan-Pearl River Delta regional economic system and the China-ASEAN Free Trade Area. In the later part of the twentieth century, the basin experienced severe droughts due to extreme precipitation shortage in 1962–1963, and suffered continuous drought for nine years between 1984 and 1992 (Wu et al. 2015; Lin et al. 2017). Since the beginning of the twenty-first century, extremely severe and long-lasting continuous droughts seem to have been frequent, especially in 2004–2006 and 2010–2014 (Han et al. 2021). The drought seriously threatens nature, quality of life, and the economy by interrupting development activities linked with water supply. Thus, the primary objectives of this study are to analyze the spatially distributed dynamics of hydrological drought in the near-real river networks based on the VIC and large-scale routing model, and to detect the possible relationship between dynamic patterns of hydrological drought and large-scale climate factors.

2 Materials and methods

2.1 Background of testing region

The Xijiang River (Fig. 1) originates from the eastern foot of the Maxiong Mountain and flows through Yunnan, Guizhou, Guangxi, and Guangdong provinces. Its watershed area is about 3.53×10^5 km² and the average annual streamflow at

the outlet Gaoyao Station is approximately $2.2 \times 10^{11} \text{ m}^3$, which is second only to that of the Yangtze River and five times that of the Yellow River in China. Its main tributaries include Beipanjiang, Liujiang, Yujiang, Guijiang, and Hejiang Rivers (Fig. 1b, c). The Xijiang basin has a humid subtropical monsoon climate with an abundant average annual precipitation between 1080 and 2760 mm (Fischer et al. 2013). However, its intra-annual distribution is heterogeneous with precipitation in the non-flood season generally accounting for only 20 to 40% of the annual amount (Niu 2013), which has resulted in severe hydrological drought and water shortage. Meanwhile, the fragile karst landforms with poor surface water retention capacity exacerbate the hydrological drought in the basin.

2.2 Distributed hydrological model

2.2.1 Variable infiltration capacity (VIC) model

The semi-distributed variable infiltration capacity (VIC) model (Liang et al. 1994) can explicitly represent the spatial-temporal sub-grid-scale variability of precipitation, infiltration, vegetation, and soil on water fluxes throughout the landscape (Meng et al. 2016). The model describes

vertical water transport with solved independent water and energy balance for each grid without lateral connectivity (Scheidegger et al. 2021). It is widely used all around the world as an open-source model. Therefore, the model structure and parameters will not be discussed here, and a more detailed description can refer to Liang's previous study (Liang et al. 1994).

In this work, VIC model version 4.2.0 was run over a regional domain of 3417 grids at a spatial resolution of 10 km with a 24-h time step in the Xijiang River basin. For each grid, the meteorological forcing data (daily precipitation, maximum, and minimum temperature) were generated by the inverse distance weighting method based on 34 meteorological stations. These meteorological datasets were obtained from the China Meteorological Data Sharing Service System (<http://data.cma.cn/>). For the underlying surface, the global 10-km soil profile dataset (Reynolds et al. 2000) and global 1-km land cover classification dataset (Hansen et al. 2000) were used to obtain the soil and vegetation parameters, respectively. Mainly seven parameters as shown in Table 1 (*B~dep3*) were required calibrations with observation data, and an auto-optimization procedure based on Rosenbrock (1960) was used under manual intervention during model calibration.

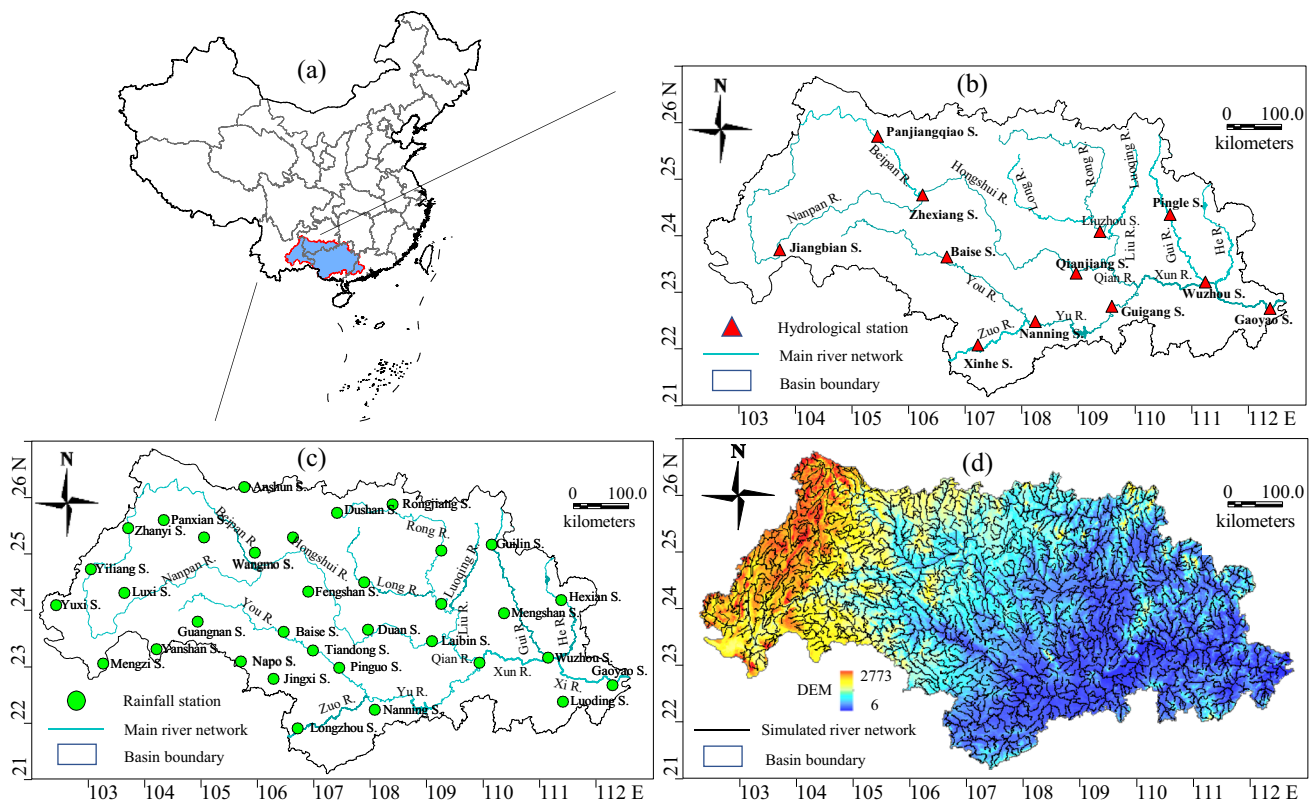


Fig. 1 Spatial distribution of **a** geographical location, **b** typical hydrological stations, **c** typical rainfall stations, **d** simulated river network generated by large-scale routing model in the Xijiang River basin

2.2.2 Large-scale routing model

The large-scale routing model (Lu et al. 2015) improves the traditional approach in river network division, slope confluence, and river network confluence based on grid and sub-basin merged unit. Firstly, the confluence paths are extracted with the high-resolution digital elevation model (DEM) and the deterministic eight-neighbor flow direction retrieval method (D8-method). Then, the point with the maximum water catchment area at the boundary of each large-scale grid and its control range (merged unit) are searched, and the routing path between points establishes the near-real river networks (Fig. 1d). Assuming that the precipitation is evenly distributed in the sub-basin merged unit, the motion wave method is conducted to obtain the outlet flow of each merged unit and then normalize it as the response function of the merged unit. Finally, the diffusion wave method is used to carry on the river routing calculation.

In this paper, the 100-m high-resolution DEM dataset was from the cloud data website of the Chinese Academy of Sciences (<http://www.csdb.cn/>). Measured daily streamflow, water surface width, velocity, and other hydrological data mainly came from the Water Resources Information Center of the Ministry of Water Resources (Lu et al 2015). Most confluence parameters can be extracted by geographic information in the routing model. Mainly two parameters, reference steady flow Q_0 and reference river width B_0 in Table 1, needed to be determined by the observed dataset. For these two parameters, the pre-existing study has given the empirical formulas in 20 geographical units of China (Wu et al. 2021).

2.2.3 Runoff simulation and validation

The initial value with manual intervention and dividing the variation range of hydrological parameters ($B \sim dep3$) is set, and then the hydrological parameters is used that change one step each time (Rosenbrock method) to run the VIC model and get the simulated runoff dataset. The above process is repeated until all the parameter combinations are tested. To assess the

model performance, the BIAS and the Nash–Sutcliffe coefficient (NSE; Nash and Sutcliffe 1970) are used to validate the effectiveness of the runoff simulation. Comparing the simulated runoff with the gauge-measured streamflow, the optimal parameter combination and simulated runoff dataset are obtained according to the optimal values of the BIAS and NSE.

In Table 2, the values of BIAS and NSE over 1961–2013 vary from -4.12 to 1.02% and from 0.73 to 0.89 , respectively. Boone et al. (2004) clarified the deterministic hydrological simulation is considered receivable if NSE is greater than 0.7 , so that the simulated results of this work are acceptable. Meanwhile, Fig. 2a–e shows the simulated hydrographs compare well with observations during multi-year continuous drought at the stations. Therefore, the runoff accuracy meets the requirements to a certain degree.

2.3 Drought analysis

2.3.1 Standardized runoff index (SRI)

Standardized runoff index was proposed by Shukla and Wood (2008). It assumes that runoff obeyed a specific distribution like precipitation and is established similar to the standardized precipitation index (SPI). Our pre-existing research found the two-parameter log-normal distribution was more suitable for establishing daily SRI in the Xijiang River basin (Wu et al. 2015; Wu and Lin 2016). Generally, the hydrological drought is classified by SRI as light drought ($-1.0 < \text{SRI} \leq -0.5$), moderate drought ($-1.5 < \text{SRI} \leq -1.0$), severe drought ($-2.0 < \text{SRI} \leq -1.5$), and extreme drought ($\text{SRI} \leq -2.0$). Figure 2f, j shows the observed and simulated SRI at the five stations during the multi-year continuous drought. It can be seen that the simulated hydrograph consists well with observations.

2.3.2 Drought characteristics

The drought characteristics used in this work are as follows: (1) The drought area A is equal to the area percentage of the

Table 1 The main user-calibrated hydrological parameters for VIC and large-scale routing model

Process	Parameter	Description	Range or function
Runoff generation (VIC model)	B	Shape parameters of infiltration capacity curve	$0 \sim 0.4$
	Dm	Maximum baseflow generated within 24 h	$0 \sim 30$ mm/day
	Ds	Proportion of baseflow in Dm when nonlinear baseflow begins	$0 \sim 1$
	Ws	Fraction of maximum soil moisture when nonlinear baseflow occurs	$0 \sim 1$
	$dep1$	Thickness of first soil moisture layer	$0.1 \sim 1.5$ m
	$dep2$	Thickness of second soil moisture layer	$0.1 \sim 1.5$ m
	$dep3$	Thickness of third soil moisture layer	$0.1 \sim 1.5$ m
Runoff routing (large-scale routing model)	Q_0	Reference steady flow	$Q_0 = \alpha_1 A^{\beta_1}$
	B_0	Reference river width	$B_0 = \alpha_2 Q_0^{\beta_2}$

Table 2 Description of sub-basin characteristics and results of daily runoff verification

Number	Station	River	Longitude	Latitude	Area (km ²)	BIAS (%)	NSE
1	Gaoyao	Xijiang	112°28'	23°03'	351,535	0.53	0.89
2	Qianjiang	Hongshuihe	108°58'	23°38'	128,938	-1.68	0.84
3	Guigang	Yujiang	109°37'	23°05'	86,333	-1.81	0.82
4	Liuzhou	Liujiang	109°24'	24°19'	45,413	-4.12	0.77
5	Pingle	Guijiang	110°40'	24°36'	12,159	1.02	0.73

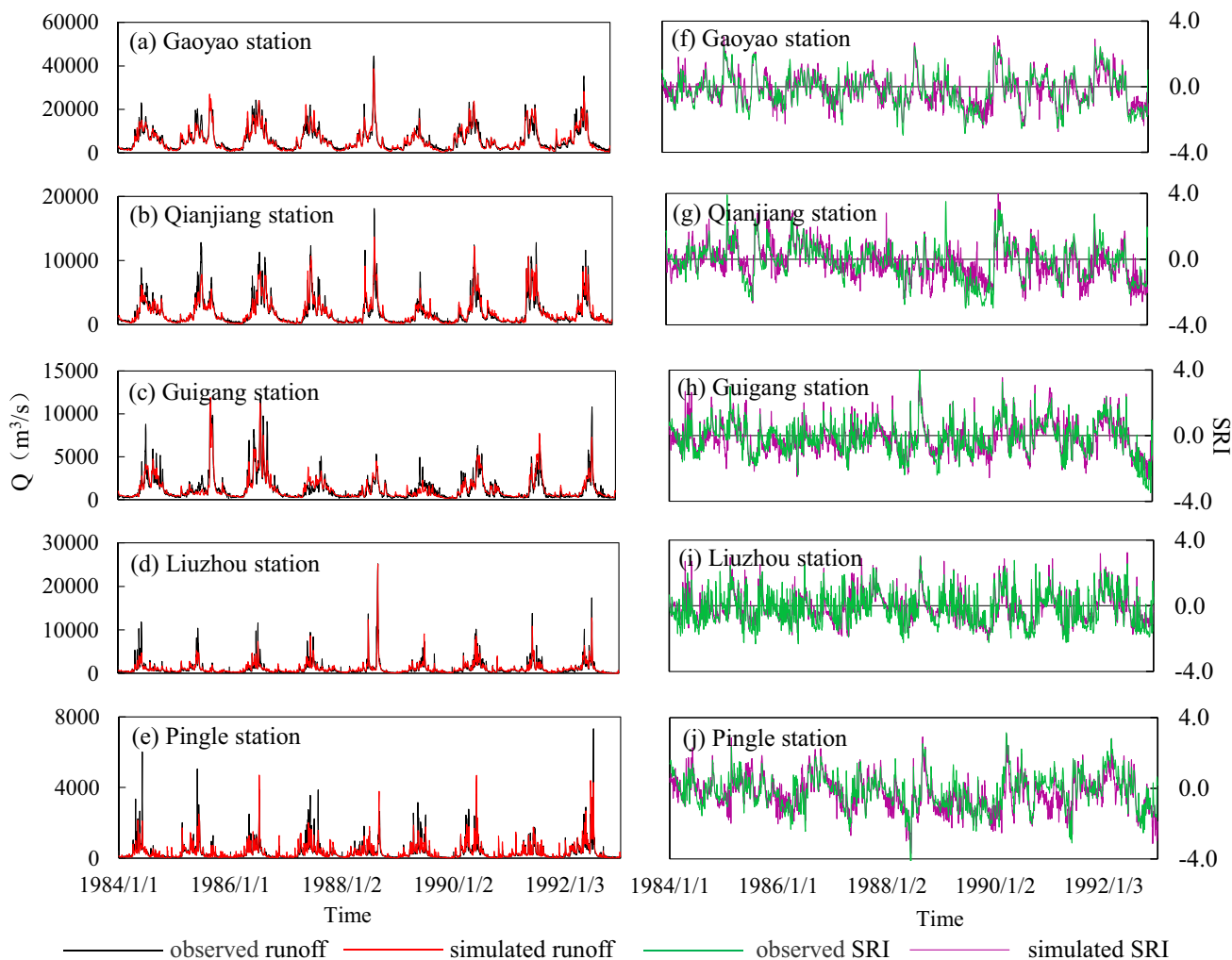


Fig. 2 Dynamic processes of observed and simulated runoff (left) and SRI (right) in five calibration stations during a multi-year continuous drought from 1984 to 1992. **a, f** Gaoyao station; **b, g** Qianjiang station; **c, h** Guigang station; **d, i** Liuzhou station; **e, j** Pingle station

region in which daily SRI is less than -0.5 . (2) The drought duration D is the continuous days of drought area A above a certain specified threshold at basin scale, or it equals continuous days of SRI less than -0.5 at grid scale. (3) Drought severity S is the accumulated value of SRI less than -0.5 of all grids in the drought period. (4) Drought intensity I is defined as the average drought severity throughout the duration (S/D).

2.3.3 Drought identification

Grid-scale drought identification needs to determine the drought duration threshold D_c and drought combined interval threshold τ_c . Basin-scale drought identification should additionally consider the drought area threshold A_c . The $D_c = 60$ days, $\tau_c = 5$ days, and $A_c = 10\%$ were

recommended for hydrological drought identification in the Xijiang River basin (Lin 2018). Based on the above thresholds, a total of 53 hydrological droughts were identified during 1961–2013 in the Xijiang River basin.

Table 3 shows the top ten worst hydrological droughts sorted by drought intensity. The 2009/2010, 1989/1990, 2011/2012, and 1962/1963 droughts were the most serious drought events. Their occurrence time, the longest-lasting durations, and the widest extension areas were consistent with the historical records, and the remaining droughts also occurred corresponded to the typical drought years (Niu and Chen 2014; Niu et al. 2015; Wu et al. 2015; Han et al. 2021). Therefore, the drought identification results are reasonable to some extent.

2.3.4 Drought concentration degree (DCD) and drought concentration period (DCP)

The construction of DCD and DCP have referred to the precipitation concentration degree (PCD) and concentration period (PCP). It is used to reveal the uneven distribution of hydrological drought within a year (Huang et al. 2018). The DCD is used to reflect the drought concentration degree within a year. It first accumulates the daily drought severity to month and annual scale, and then conducts vector calculation with monthly azimuth to get vector sum. The ratio of the vector sum to the annual severity is the concentration degree. DCP refers to the vector azimuth after the severity vector is synthesized. It is used to reflect the month in which the drought is concentrated. The detailed formulas of DCD and DCP are in the Appendix.

2.3.5 Drought intensity-area-frequency (I-A-F) curve

The drought curves are used for the visualization and interpretation of regional droughts (Henriques and Santos 1999). In recent years, the severity-area-frequency (S-A-F) curve has been widely used and has proven well express the multi-variable characteristics of regional drought (Ahmed et al. 2019; Li et al. 2020a, b; Kumar et al. 2021). Referring to the S-A-F curve formulation process suggested by Mishra and Desai (2005) and Mishra and Singh (2009), the I-A-F curve was constructed by replacing drought severity with drought intensity. In this work, the joint frequency of drought intensity and area under fixed drought durations were calculated with the Frank Copula function, for previous research based on gauge streamflow shows the Frank Copula was the best fitting function in the Xijiang River basin (Wu et al. 2015).

2.3.6 Teleconnection analysis

The Pearson correlation coefficient (Nahler 2009) was used to discuss the relationship between hydrological drought and teleconnection factors. Teleconnection data from 1961 to 2013 came from the US National Oceanic and Atmospheric Administration (<http://www.noaa.gov/>), including the monthly data of the Atlantic Multidecadal Oscillation (AMO), El Niño Southern Oscillation (ENSO), Pacific Decadal Oscillation (PDO), and Arctic Oscillation (AO), which affect global and regional climate by influencing the exchange process of the mass, momentum, and heat in the atmosphere.

2.4 Study period division

To evaluate the evolution dynamics of hydrological drought, five parametric or nonparametric test methods were used to divide the study period, including the moving

Table 3 Statistics of typical hydrological drought variables based on drought identification thresholds at basin scale

Number	Period	Duration (days)	Area (%)	Average drought intensity (SRI/day)	
				Grids in drought	All grids
1	2009/08/06~2010/06/09	308	66.6	1.15	0.77*
2	1989/05/31~1990/03/12	286	67.2*	0.97	0.65
3	2011/05/14~2012/06/11	395	51.9	1.21*	0.63
4	1962/10/15~1963/11/23	405*	59.6	0.95	0.56
5	1998/09/15~1999/05/07	235	60.7	0.87	0.53
6	1992/07/27~1993/05/01	279	63.7	0.81	0.52
7	2004/07/31~2005/06/04	309	59.6	0.78	0.46
8	1987/12/16~1988/08/28	257	44.7	0.62	0.46
9	2012/08/08~2012/11/15	100	40.1	0.61	0.46
10	1991/04/01~1991/06/20	81	54.3	0.82	0.44

(The symbol * stands for maximum value)

t , Cramer, Yamamoto, Lepage, and Mann–Kendall test (Zhang 2014). Their formulas are shown in the Appendix. The mutation years of annual drought severity detected by above methods were 1982, 2006, 1982, 1980/1982, and 1983, respectively. Thus, droughts mutation mainly occurred during 1980–1983. Due to pre-existing study proposed that precipitation in Guangxi province experienced a sudden decline in 1984 (Li and Su 2009), so the period from 1961 to 2013 was divided into 1961–1983 and 1984–2013 in this work.

3 Results

3.1 Spatial–temporal dynamics of hydrological drought

To reveal the dynamics of droughts that may be disastrous due to long-term water shortages in the river, the hydrological droughts that lasted more than 60 days in the grid were selected to explore the spatial distributions of drought number, duration, severity, and intensity (Fig. 3).

In Fig. 3a, the average drought number in the Xijiang River basin was 0.5 times/year, and the river length proportion in which the drought number exceeded the average was 61.1%. These reaches were primarily located in the middle-lower regions, including tributary Liujiang, Guijiang, and Hejiang River basins. The spatial evolutions of drought duration and severity in Fig. 3b, c were similar. The average drought duration \bar{D} and severity \bar{S} were 143 days and 90.7 SRI, and the river length proportion with \bar{D} exceeding 120 days and 180 days were 66.3% and 15.8%, respectively. The maximum average drought duration \bar{D}_{\max} was 610 days; that is, each drought lasted more than 1.5 years. The upstream region, Nanpanjiang, Beipanjiang, Youjiang, and Duliujiang sub-basins had experienced long-lasting and high-severity droughts. In Fig. 3d, the average drought intensity \bar{I} was relatively high in the middle region and the river length proportion in which \bar{I} exceed 0.5 SRI/day was 82.9%. The \bar{I} in the mainstream was more prominent than that in the surrounding region, and that in Nanpanjiang River even exceeded the severe level.

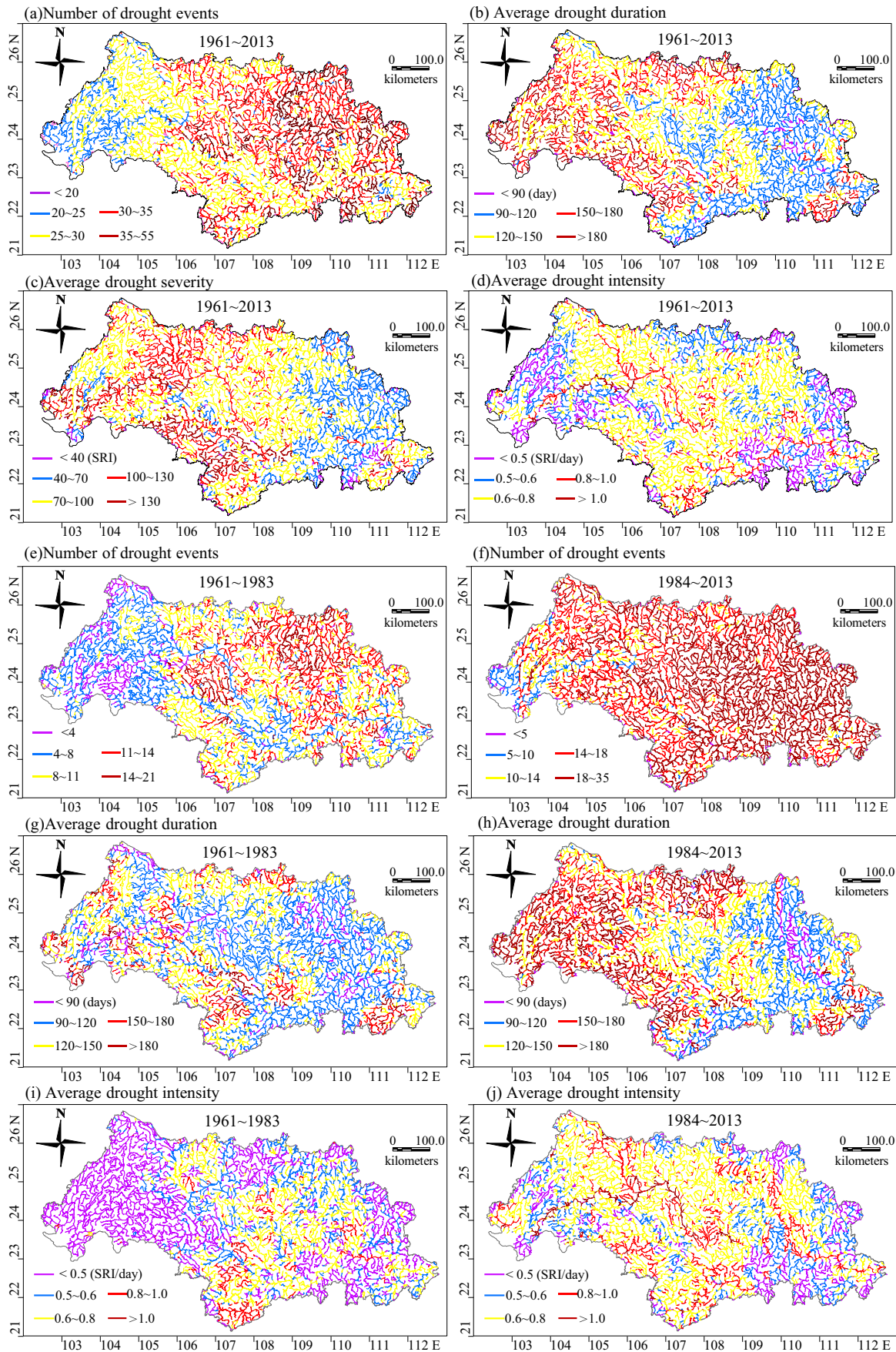
Figure 3e–j shows the different drought dynamics before and after mutation. The drought number in the figure uses different classification levels in two different length periods so that the coincident color represents the same drought frequency. In Fig. 3e, f, the average drought numbers were 0.47 and 0.69 times/year from 1961 to 1983 and 1984 to 2013, respectively. The river length proportion with drought number exceeding 0.5 times/year increased from 32.7 to 86.0%. The increased trends existed in the whole basin, especially in the Yujiang River basin and middle-lower reaches of the

Xijiang River basin. The river length proportions in which \bar{D} exceeding 120 days and 180 days increased from 44.9 to 72.0%, and from 5.8 to 23.6%, respectively. Accordingly, the river length proportion in which \bar{I} exceeding 0.5 SRI/day increased from 54.0 to 87.6%. The growth rate was 62.2% and the growing majority arose in the upstream.

From the perspective of the drought spatial distributions, there was a saddle-shaped evolution from 1961 to 1983 with northeast-southwest as the ridge (high-value region) and northwest-southeast as the saddle (low-value region). However, drought characteristics had changed from 1984 to 2013, and the saddle shape of drought relief had disappeared. The drought numbers increased substantially across the whole basin, and long-duration droughts significantly increased in the upper reaches. Similar to the annual dynamics of hydrological drought, the distributions of drought within a year may be altered under the changing background. Therefore, the drought concentration degree (DCD) and drought concentration period (DCP) were investigated, and the results were shown in Fig. 4.

In Fig. 4d, the drought was mainly concentrated in the summer from 1961 to 2013. Specifically, the drought mainly concentrated in July in the upstream, and that in the downstream was generally delayed a month. In Fig. 4e, f, the droughts mainly concentrated in summer during two different periods. Unlike in 1961–1983, the droughts in the eastern part of the basin (Hejiang and Guijiang River basins) mainly occurred in autumn during 1984–2013. Therefore, the regional drought likely showed a delay tendency from summer to autumn under the changing background. What is more, the river length proportion in which drought concentrated in autumn reached 41.2% when coming to twenty-first, the delay phenomenon becoming more pronounced. Li et al. (2010) analyzed the variation characteristics of meteorological drought from 88 stations in Guangxi province during 1961–2009, and pointed out that the drought index and disaster area showed an increasing tendency, especially in autumn. The season synchronization of hydrological drought and meteorological drought revealed that the delay tendency might be mainly affected by precipitation.

Drought frequency is as essential as drought deficit in drought research. An I-A-F curve is a good tool for understanding drought multivariate frequency. Herein, the fixed drought durations D ($D = 60, 90, 120, 150, \text{ and } 180$ days) were employed to obtain drought samples. For example, the number of drought samples that lasted 60 days, 90 days, and 120 days during a drought event that continued for T days were T-60, T-90, and T-120, respectively. Accordingly, the number of drought samples from 1961 to 2013 under the above five fixed durations were 4344, 3072, 2262, 1760, and 1347 in the Xijiang River basin, respectively. The statistical



◀**Fig. 3** Spatial distribution of average drought number (a, e, f), drought duration (b, g, h), drought severity (c), and drought intensity (d, i, j) in different periods

results of drought intensity corresponding to different drought areas were displayed in Fig. 5.

Figure 5 shows the average value and the variation range of drought area and drought intensity at different drought development stages. In the figure, the drought area generally exceeds 50% when the drought lasted for more than 5 months, and when the drought area was around 70%, the drought intensity usually reached the

maximum across the basin. When D equaled 90 days and the areas equaled 60%, 70%, and 80%, respectively, the maximum average drought intensities of top-severe hydrological drought events (2009/2010, 1989/1990, 2011/2012, 1962/1963) were 0.85, 0.99, and 0.93, which were lower than 0.88, 1.07, and 1.02, which were the upper boundary values of the curve. Therefore, the extreme values did not appear in the most extreme events in the past, and the basin may experience more severe droughts along with extreme values in the future. On the multivariate basis of drought variables, the joint

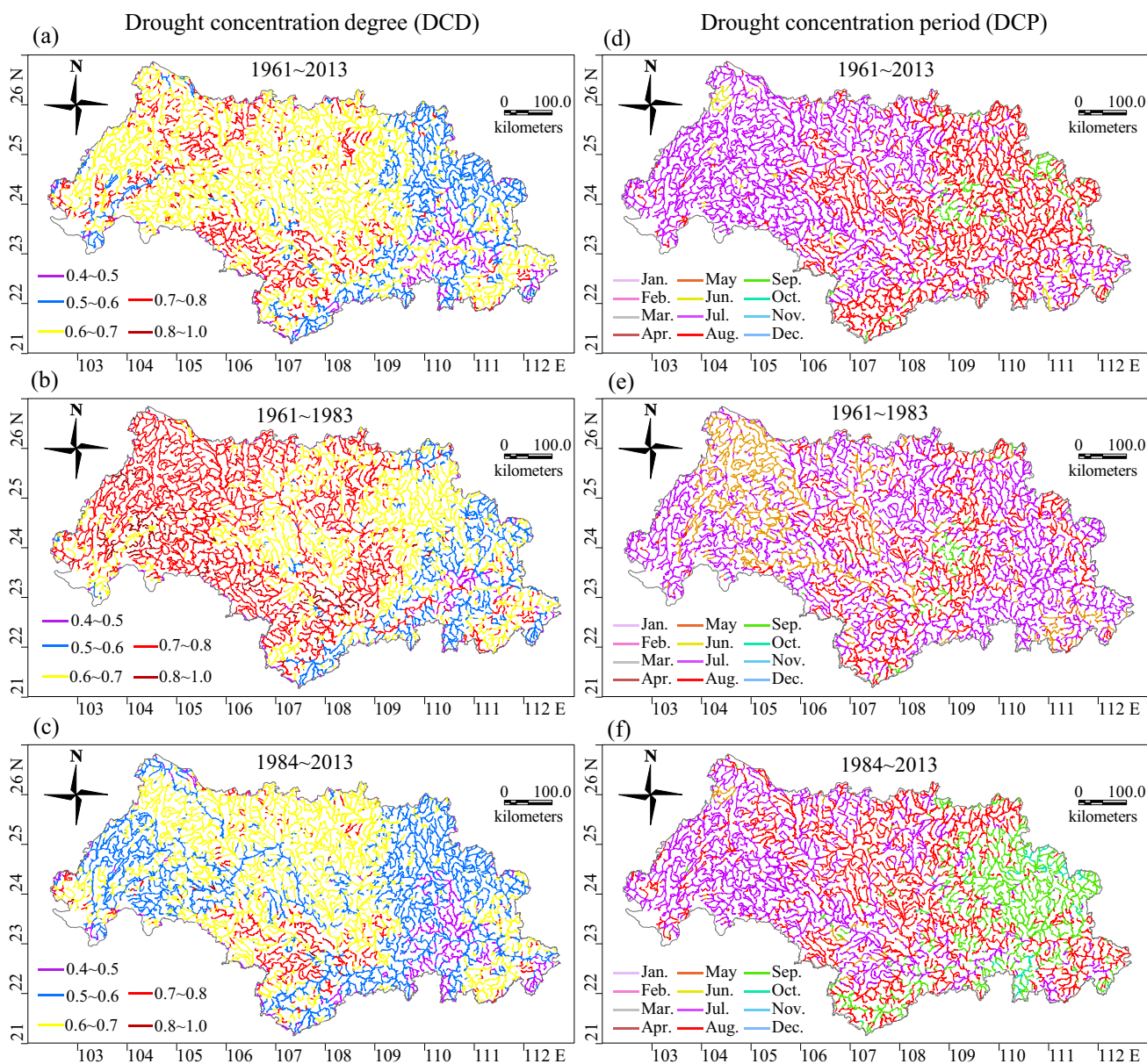


Fig. 4 Spatial distribution of hydrological drought concentration degree (DCD) (a, b, c) and drought concentration period (DCP) (d, e, f) in different periods

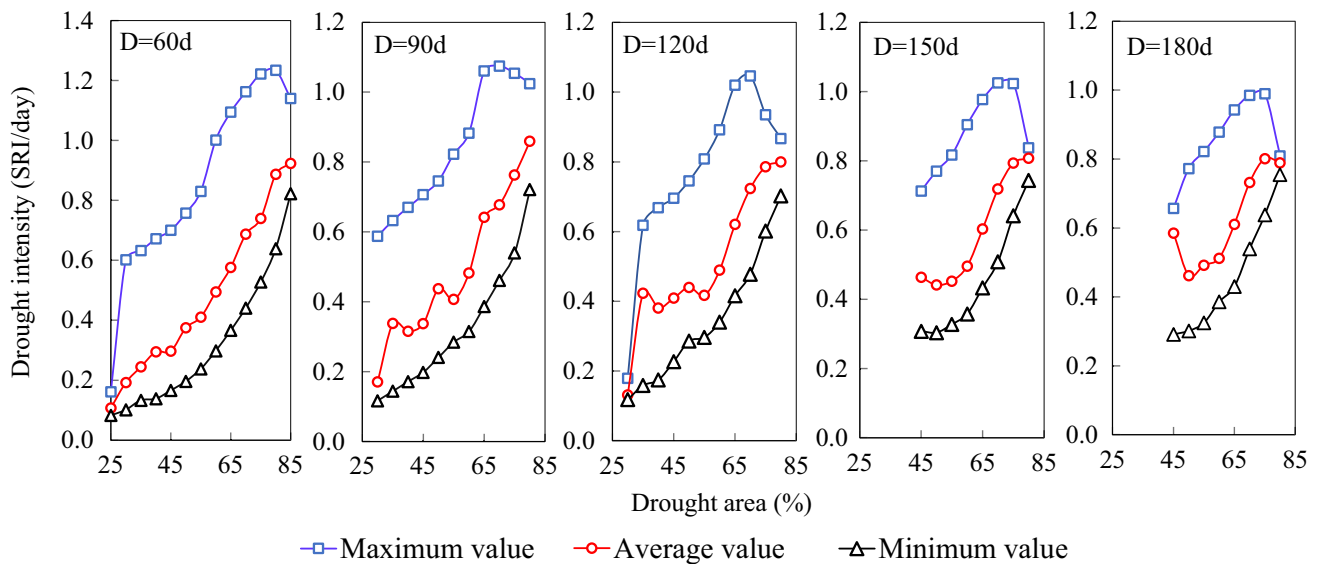


Fig. 5 Multivariate association characteristics of drought area and drought intensity under fixed drought duration (D) from 1961 to 2013

frequency was calculated with the Frank Copula function and the I-A-F curve was shown in Fig. 6.

Figure 6a shows the joint frequency of drought area and intensity with four fixed drought durations. When the drought durations were 60 days and 90 days, the distances between the frequency contours were relatively uniform, and when durations increased to 120 days and 150 days, the contours tended to be dense with the upward shift of low-frequency curves. Figure 6b, c shows the comparative effect between the joint frequencies of two different periods. The frequency evolutions of the latter period were similar to that of the whole sequence because severe drought samples were mostly obtained in the latter period. If a drought sample was put into two periods and individually calculated the joint frequency, the value was smaller in the period 1983–2014. For example, if drought area and intensity were 60% and 0.6 SRI/day, when fixed durations equaled to 60, 90, 120, and 150-days, the joint frequency were 0.76, 0.68, 0.54, and 0.35 in 1961–1983, and that of 1984–2013 were 0.47, 0.35, 0.25, and 0.19, respectively. It can be seen that the same drought ranked lower in the later period for more severe droughts surpassing it. Therefore, the drought risk increased in the latter period under the changing background in the Xijiang River basin.

3.2 Dynamic pattern-testing of hydrological drought

The above sections revealed the drought dynamics from the single aspect of drought variables, but drought variables are generally not changing individually. In view

of this, we have chosen four variables of drought intensity, drought concentration degree, drought concentration period, and drought frequency to observe which variable or their combination was the main direction of drought change, so as to take different countermeasures. The reason why these four variables were chosen was that precipitation amount, concentration degree, concentration period, and frequency are often selected in the study of precipitation dynamics (Chatterjee et al 2016), which are considered to be effective indicators for evaluating the change direction of precipitation. As a natural hazard, the dynamic direction of drought is also essential for its prevention.

The four drought variables altogether consist 16 dynamic patterns in Table 4, including no significant changes in any variables (S0), each variable changes significantly (S1~S4), any two variables change significantly (S5~S10), any three variables change significantly (S11~S14), and four variables all change significantly (S15). The significant change means that the variable increase or decrease trend has passed the 0.05 significance test with the MK method.

The grids number rather than the river length ratio was used as the statistical variable in Table 4 to directly represent the statistical results. In the table, the Xijiang River basin had the greatest grid ratio in the S0 pattern, approximately accounting for 49.8%. The grid ratio with the significant change of at least one variable was 50.2%, slightly greater than that had no significant change. The proportion of only one variable with significant change was 15.5%, and most of them were in the S1 pattern. The ratio of simultaneous changes of the two variables was 16.9%,

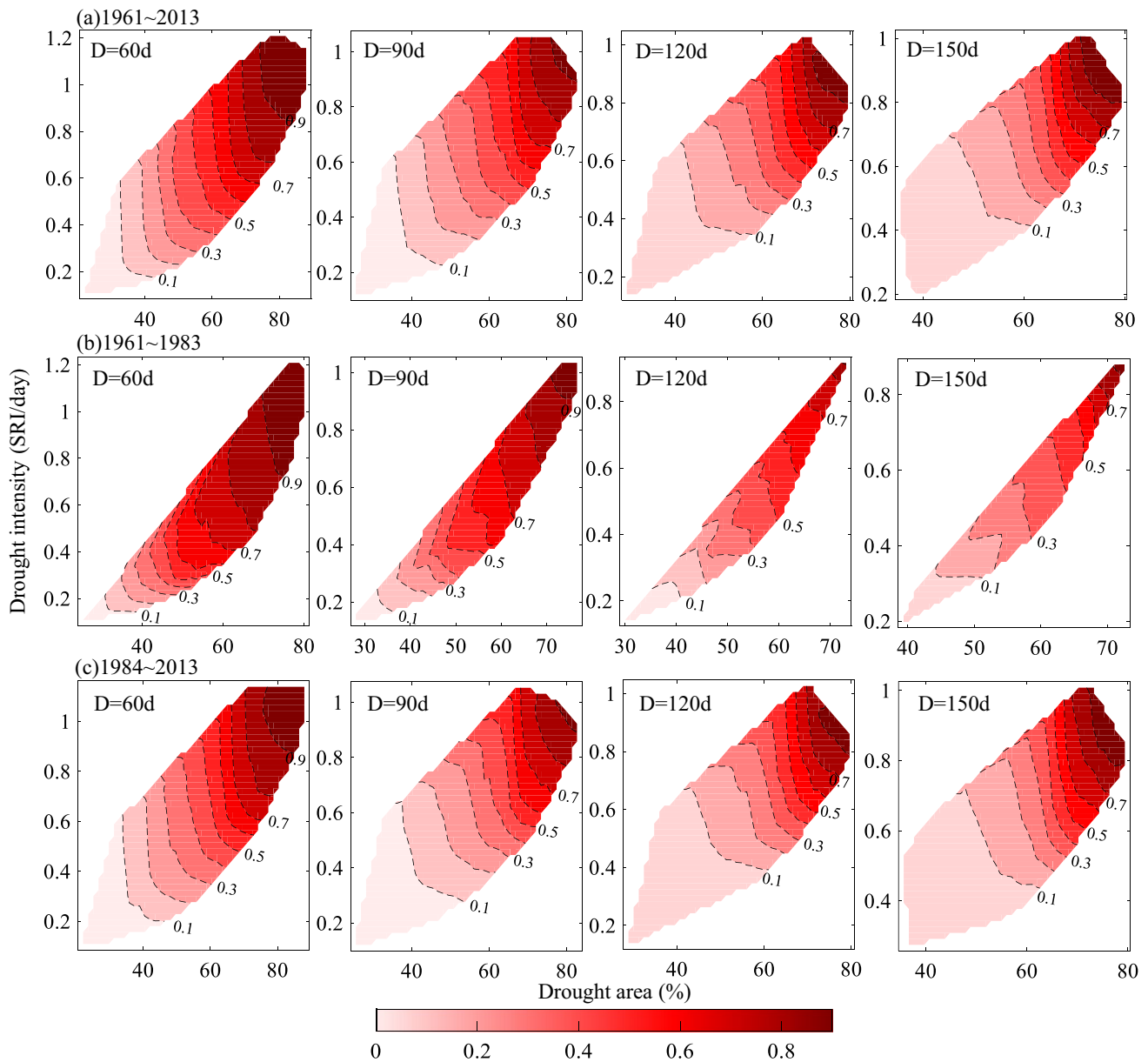


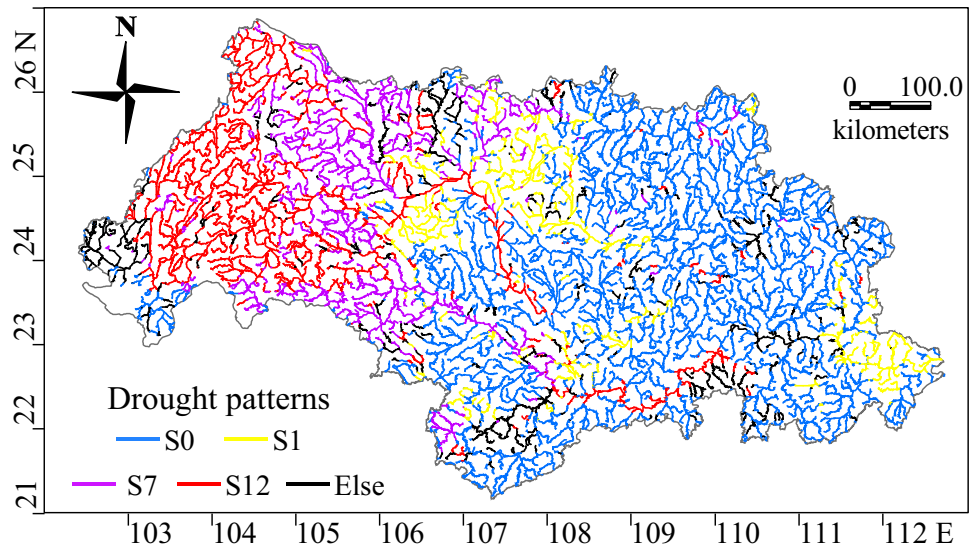
Fig. 6 Intensity-area-frequency (I-A-F) curves of hydrological droughts under fixed drought duration (D), dotted line indicates the joint frequency. **a** 1961~2013, **b** 1961~1983, **c** 1984~2013

among which the S7 pattern was more common. Similarly, the ratio of the three variables changing simultaneously was 17.7%, almost all occurring in the S12 pattern. However, there were few rivers in which four variables changed simultaneously.

Since drought is a large-scale natural disaster occurring in contiguity, the scattered information has little significance for drought prevention and control. Therefore, only primary dynamic patterns S0, S1, S7, and S12 are separately shown in Fig. 7. The other patterns were put into the “Else” category. In spatial, the pattern S0 mainly existed in the middle-lower rivers of the basin, and the rivers with at least

one variable significantly changing were mainly located in the upstream, including Nanpanjiang, Beipanjiang, Hongshuihe Rivers, and Yujiang mainstream. The pattern S1 was mainly located in the regions between Hongshuihe and Liujiang River basins, pattern S7 mainly appeared in the upper reaches of Beipanjiang and Yujiang River basins, and pattern S12 mainly arose in the Nanpanjiang River basin and the Hongshuihe mainstream. In summary, the hydrological drought was mainly manifested as intensity-concentration-frequency joint variation (S12), the intensity-frequency joint variation (S7), and the intensity-independent variation (S1) in the upper reaches of the Xijiang River basin.

Fig. 7 Spatial distribution of typical combination patterns of drought variables from 1961 to 2013, the pattern settings are listed in Table 4



3.3 Association with the large-scale climate indices

This section investigates the possible links between hydrological drought and climate evolutions with correlation analyses. Referring to the teleconnection analysis of hydro-meteorological variables in the Xijiang River basin in pre-existing studies (Lin et al. 2017; Li et al. 2020a, b; Liu et al. 2020), four major low-frequency climate factors (AMO, ENSO, PDO, and AO) were chosen to construct 16 variability patterns in Table 5. The pattern-setting ways are similar to that in Table 4. The correlation coefficient CC values between annual drought variables and climate factors (warm phase and cold phase) were calculated, and the grid number in which CC pass 0.05 confidence was counted.

In Table 5, the warm phase of low-frequency climatic variability factors showed a greater influence on drought than that of the cold phase. The drought variables affected by climate factors in descending order were drought

frequency, drought intensity, drought concentration degree, and drought concentration period, and the grid ratios of at least one of the warm phases had an effect on them were 59.9%, 53.0%, 49.2%, and 20.0%. The corresponding ratios of cold phase were 30.0%, 38.2%, 29.0%, and 11.9%, respectively. The grid ratios of only one of the warm phases had an effect on them were 51.9%, 43.4%, 41.1%, and 18.6%, and the main pattern was M1. The corresponding ratios of the cold phase were 28.7%, 29.6%, 27.0%, and 10.9%, respectively. For the cold phase, the main patterns that affected drought intensity were M3 and M1, and that affected drought concentration degree and frequency were both M1. The proportions of two climatic factors simultaneously affecting drought factors were less than 10%, and that of three or more climatic factors simultaneously affecting drought was almost negligible.

Figure 8 shows the spatial distribution of primary combination patterns of climate variability factors. Only the

Table 4 Dynamic patterns setting and statistic results of grid numbers for each pattern

Patterns	Significant change factors				Number of 10-km grids	Patterns	Significant change factors				Number of 10-km grids
	DI	DCD	DCP	DF			DI	DCD	DCP	DF	
S0					1700	S8	√		√		14
S1	√				319	S9		√		√	45
S2		√			52	S10			√	√	3
S3			√		49	S11	√	√	√		0
S4				√	110	S12	√	√		√	603
S5	√	√			38	S13	√		√	√	1
S6	√		√		2	S14		√	√	√	1
S7	√			√	474	S15	√	√	√	√	6

(DI, drought intensity; DCD, drought concentration degree; DCP, drought concentration period; DF, drought frequency)

top five patterns were separately listed and the relatively small patterns were categorized into the “Else” category. It can be seen that climatic variability factors mainly affect the hydrological drought in the upstream, but have little effect on the drought concentration period across the basin. In particular, drought intensity was primarily affected by warm M1, warm M7, and cold M3 patterns in the upper reaches. The drought frequency and concentration degree were mainly affected by both warm and cold M1 patterns. In the downstream, the concentration degree of Liujiang and Guijiang River basins were still affected by the warm M2 pattern. In general, the drought in the upper reaches of the Xijiang River basin was mainly influenced by both warm and cold AMO. The effects of cold PDO and warm AMO/AO also deserve attention in the upper reaches of the Beipanjiang River basin.

4 Discussion

4.1 Effects of meteorological, topographic, and river network structure on hydrological drought dynamics

Hydrological drought is generally characterized as the streamflow deficit. Zhang (2012) studied the influence of meteorological factors on streamflow in the Xijiang River basin and proposed that precipitation is the most important factor affecting streamflow, followed by evaporation. Other climatic factors (such as relative humidity, diurnal temperature range, sunshine duration) indirectly affect streamflow mainly through affecting precipitation and evaporation. Meanwhile, several pre-existing studies have analyzed the spatial distribution of meteorological drought in the Xijiang River basin based on standardized precipitation index SPI and standardized precipitation evapotranspiration index SPEI, and proposed that meteorological drought in the higher terrain areas in the northwest (mainly concentrated in the border area of Yunnan province and Guizhou province) show a significant upward trend (Zhang and Li 2018; Li et al. 2020a, b), which is consistent with the drought tendency in Fig. 7. Therefore, precipitation is the main factor affecting hydrological drought compared with other meteorological factors.

The long-duration and high-intensity droughts were mainly located in the upper reaches of Xijiang River basin, which is closely related to topography. In particular, the CC between altitude and the trend value of drought frequency, severity, and intensity are 0.67, 0.56, and 0.51, respectively, which are moderate correlations. Nevertheless, the CC values between slope and various drought variables are less than 0.2, and that for aspect

is similar. Therefore, the large-terrain effect on hydrological drought is stronger than that of micro-terrain. The large topography has an obvious blocking effect on water vapor. The water vapor from the Bay of Bengal and the Indian Ocean could not be transported to the upper reaches of the Xijiang River due to tall terrain barriers. In addition, the Fohn effect caused by the tall terrain may enhance the drought in the upper reaches of the Xijiang River basin.

The long-distance propagation of hydrological drought in the mainstream is obvious in several figures (e.g., Fig. 3c, d), and it is more outstanding in the downstream of Nanpanjiang, Beipanjiang, and Yujiang Rivers. This phenomenon is not only related to the complex topography, but also may have relevant to the river network structure of sub-basins. The Nanpanjiang and Yujiang sub-basins have a long-scattered river network structure, which enhances the memory time of streamflow to precipitation shortage. Therefore, the transmission distance of drought in the downstream river is relative far. The Liujiang River and Guijiang River basins have fan-shaped watersheds and converge-type river networks, which will maintain more high-frequency precipitation variability, and the short-term recovery of precipitation will alleviate the drought. As a result, hydrologic drought in narrow river network structures spreads over longer distances than the fan-shaped basin.

4.2 Influence of Atlantic Multidecadal Oscillation on hydrological drought

The main mechanism of AMO affecting the climate in the Asian monsoon region is that AMO changes the thermal and baric gradient difference between land and sea by heating the middle and upper troposphere over Eurasia (Ding et al. 2020; Zhu et al. 2021). Several pre-existing studies have shown that the North Atlantic SST anomaly may change temperate, monsoon, and drought in East Asia. Li and Bates (2007) have modeled multiple atmospheric circulations and found that the warm AMO corresponds to the warm winter in most parts of China, resulting in less rain in the south and more rain in the north of China. Wang et al. (2009) indicated that warm AMO not only corresponded to the warm winter, but also contributed to the warming of East Asia in all seasons. Qian et al. (2014) revealed the North Atlantic SST anomalies could change oceanic-atmosphere-land surface interaction processes and directly affect the local climate in eastern Asia. The above studies reveal that although the North Atlantic is far away from eastern Asia, the SST anomaly will cause local climate change, which is consistent with the conclusion of this work.

Our pre-existing research result (Lin et al. 2017) based on the gauge streamflow of the Gaoyao station revealed

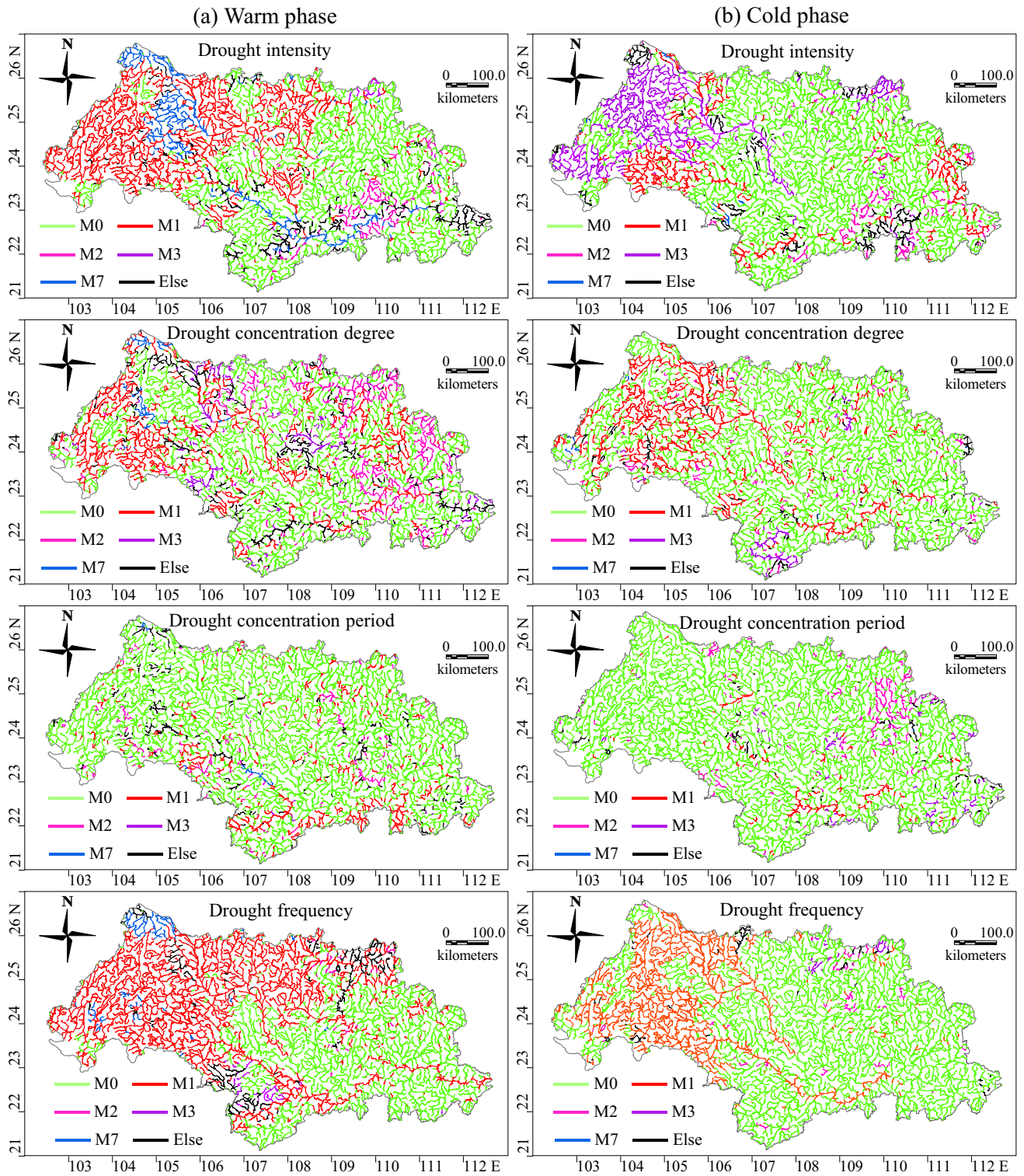


Fig. 8 Spatial distributions of typical combination patterns of climate variability factors that significant relation with hydrological drought, the pattern settings are listed in Table 5. **a** Warm phase, **b** cold phase

Table 5 Patterns setting of climate factors and statistical numbers of grids in which drought variables significant related to climate indices ($\alpha=0.05$)

Patterns	Climate variability factors						Number of 10-km grids in patterns					
	AMO	ENSO	PDO	AO	DI		DCD		DCP		DF	
					Warm phase	Cold phase	Warm phase	Cold phase	Warm phase	Cold phase	Warm phase	Cold phase
M0					1605	2113	1737	2427	2733	3009	1370	2393
M1	√				1129	381	783	724	371	105	1692	885
M2		√			148	128	410	103	126	166	25	68
M3			√		19	384	135	68	15	73	41	20
M4				√	187	118	77	26	123	30	17	6
M5	√				41	8	42	42	24	10	123	31
M6	√			√	7	176	105	1	2	2	58	0
M7	√			√	250	12	45	12	13	1	87	1
M8		√		√	14	96	41	12	0	17	0	13
M9		√		√	4	1	8	1	8	1	0	0
M10				√	2	0	6	0	1	1	0	0
M11	√			√	0	0	27	1	0	1	2	0
M12	√	√		√	2	0	0	0	1	1	2	0
M13	√			√	9	0	0	0	0	0	0	0
M14		√		√	0	0	1	0	0	0	0	0
M15	√	√		√	0	0	0	0	0	0	0	0

(DI, drought intensity; DCD, drought concentration degree; DCP, drought concentration period; DF, drought frequency)

that among four low-frequency climate variability factors, ENSO has the highest correlation with hydrological drought events, while AMO shows the highest correlation with drought in this work. The reasons why inconsistent conclusions formed are as follows: firstly, previous studies described the significant correlation between ENSO and intermittent severe drought events based on the cross-wavelet analysis, while this work explored the correlation coefficient between the whole time series. The total sequence correlation of AMO and drought is stronger than that of ENSO, but its effect on severe drought events is weaker than ENSO. Secondly, the climate pattern that has a significance relationship with drought intensity in the grid of Gaoyao station in Fig. 8 is the M5 pattern, that is, affected by both warm AMO and ENSO. However, when only used outlet gauge streamflow to represent hydrological drought, the impact of AMO in the upper reaches has been ignored because it cannot transmit to the outlets.

4.3 Limitations of drought monitoring based on sparse stations for the large watershed with complex topography

In Fig. 3c, d, the average transfer endpoint of severe droughts in the upper main river is generally located at 108° 39' E, 23° 42' N. Although the transmission distance is long, but is only about half the length of the mainstream, the downstream gauges could not receive drought shortage signal. At this time, drought monitoring based on the sparse gauge is easy to miss the drought in the complex topographic area of the upstream. Taking two typical droughts that mainly occurred in the upper reaches as examples, the peak times of 2009/2010 and 2011/2012 droughts monitored by outlet gauge Gaoyao were in October 2009 and September 2011, which by model simulation were in March 2010 and March 2012, respectively. Referred to the pre-existing research results, the simulated drought was more consistent with the actual drought in processes and peak times (Niu et al. 2015; Yuan et al. 2021). Therefore, the hydrological drought can be studied with outlet gauge streamflow in a small watershed or basin with simple topography, as is done in most studies. However, it is suggested to conduct drought simulation in a large watershed with complex terrain.

4.4 Research prospects

The VIC model in this paper does not consider the human interference module due to the difficulty of data acquisition. However, anthropogenic activities such as hydropower generation, deforestation, urbanization, and population growth can directly impact hydrological drought (Yuan et al. 2017). Wada et al. (2013) concluded that human activities are one of the most important mechanisms that exacerbate hydrological drought and may continue to be the main

factor affecting the intensity and frequency of drought in the future. Margariti et al. (2019) found that human activities increase drought termination rates in all case studies of Europe. Rangelcroft et al. (2019) determined that, due to the establishment of the reservoir, hydrological drought was aggravated, and the drought duration and drought intensity increased in the downstream area of the Huasco basin in the arid region of northern Chile. Therefore, factors with strong human interference such as reservoir and vegetation can be incorporated into the VIC simulation in further studies, and non-stationary drought parameters can be constructed to improve the monitoring accuracy of human-disturbed drought in the Anthropocene. In addition, the distributed routing model generates the near-real river network, and river characteristics such as deficit river length can be used to replace the drought area to identify drought events, so that the calculation weight is greater in areas with dense river networks, which is beneficial for refining expression of hydrological drought.

Global climate change will inevitably lead to the variation of the water cycle and the spatial–temporal re-distribution of water resources. Pre-existing studies analyzed the future daily precipitation with different climate patterns and proposed that precipitation in the dry season would decrease, while the annual and monthly mean temperatures would increase significantly in the Xijiang River basin (Shan et al. 2016; Touseef et al. 2020). Therefore, the hydrological drought dynamics under future climate patterns can be studied based on the VIC and large-scale routing model to analyze the drought condition in advance.

5 Conclusions

In this study, the dynamics and patterns of the hydrological drought in the near-real river networks were investigated based on the VIC and large-scale routing model, and its relationships with large-scale climate factors were discussed in the Xijiang River basin. The main results are summarized as follows:

(1) The constructed VIC and large-scale routing model can meet the accuracy requirements of runoff simulation in the Xijiang River basin. Simulated continuous daily runoff series based on grid and sub-basin merged units have low absolute BIAS ($\leq 4.12\%$) and high NSE (≥ 0.73), and the simulated river networks are close to real networks. Based on simulated runoff and the SRI index, the spatial–temporal dynamics of hydrological droughts in near-real river networks were well revealed, especially showing the downward transfer phenomenon of drought in main river channels.

(2) The spatial–temporal dynamics of hydrological drought before and after mutation were compared. The drought risk increased significantly based on the I-A-F curve in the latter period 1984–2013. Specifically, the length proportion of rivers in which drought number exceeds 0.5 times/year significantly

increased from 32.7 to 86.0% across the whole basin, the average drought duration surpassed 120 days and drought intensity exceeded 0.5 SRI/day increased by 60.4% and 62.2%, respectively. After 1983, the summer drought in the lower reaches was mostly delayed to be the autumn drought, and the delay tendency in the 2000s is more significant.

(3) The comprehensive dynamic patterns of drought intensity, concentration degree, concentration period, and frequency were revealed. The grid ratio with the significant change of at least one variable was 50.2%, and that of one to three variables simultaneously changed were 15.5%, 16.9%, and 17.7%, respectively. The significant changes are mainly located in the upper reaches and manifested as three combination patterns: S12 (simultaneous significant changes in drought intensity, concentration degree, and frequency), S7 (simultaneous significant changes in drought intensity and frequency), and S1 (single significant change in drought intensity).

(4) The relationships between hydrological drought and large-scale climate indices were revealed. The correlation with climate factors from great to small are drought frequency, intensity, concentration degree, and concentration period. The grid ratios of above drought variables associated with warm phases of climate factors were 59.9%, 53.0%, 49.2%, and 20.0%, which associated with cold phase were 30.0%, 38.2%, 29.0%, and 11.9%, respectively. The hydrological droughts in the upper reaches were mainly related to patterns M1 (warm and cold AMO), partial regions are related to patterns M3 (cold PDO) and patterns M7 (warm AMO/AO).

Appendix

Drought concentration degree (DCD) and Drought concentration period (DCP)

Referring to the concepts of precipitation concentration degree and concentration period, the calculation formula of drought concentration degree, and concentration period is as follows:

$$C_i = \frac{\sqrt{S_{xi}^2 + S_{yi}^2}}{S_i} \tag{1}$$

$$P_i = \arctan\left(\frac{S_{xi}}{S_{yi}}\right) \tag{2}$$

$$S_{xi} = \sum_{j=1}^N s_{ij} \times \sin\theta_j \tag{3}$$

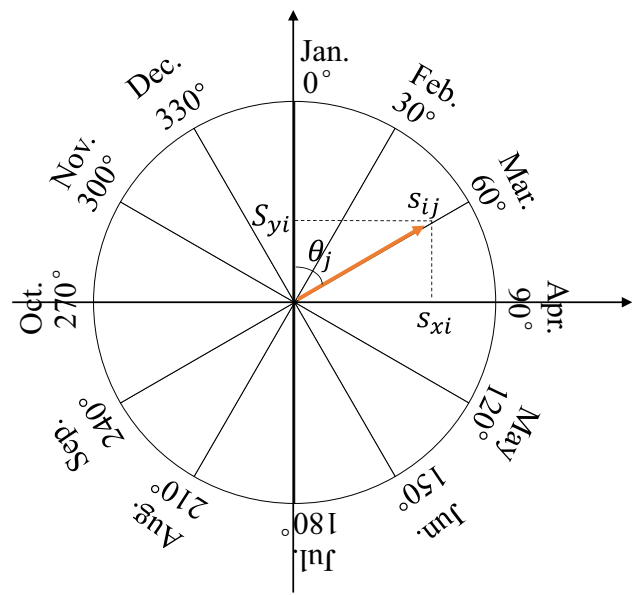


Fig. 9 The representative degree θ_j of each month

$$S_{yi} = \sum_{j=1}^N s_{ij} \times \cos\theta_j \tag{4}$$

where i is the year, j is the month. C_i and P_i are the concentration degree (DCD) and concentration period (DCP) of hydrological drought in the year, respectively. S_i is the drought severity of year i , and s_{ij} is the drought severity of month j in the specified year i . The s_{xi} and s_{yi} represent the horizontal and vertical components of the vector s_{ij} . The θ_j is the representative degree of each month (Fig. 9), e.g., the θ_j of January and February are 0° and 30° . After vector calculation, the P_i has different values. When the P_i falls between $15^\circ \sim 45^\circ$, it means that drought concentrates in February, and the angle range of other months can be analogized in turn.

Moving t-test method

The criterion of the moving t -test is whether the significant difference exists in sequence means. If the time series x has n variables, a certain time can be arbitrarily set as the test cut-off point, and the sequence sizes of sub-sequence x_1 and x_2 before and after the cut-off point are n_1 and n_2 , the mean values are \bar{x}_1 and \bar{x}_2 , and the variances are s_1^2 and s_2^2 , respectively.

$$t = \frac{\bar{x}_1 - \bar{x}_2}{s\sqrt{\frac{1}{n_1} + \frac{1}{n_2}}} \tag{5}$$

$$s = \sqrt{\frac{n_1 s_1^2 + n_2 s_2^2}{n_1 + n_2 - 2}} \tag{6}$$

The sliding method is used to set the cut-off points and the responding statics t_i are calculated. The critical value t_α can be obtained with a given significance level. If $|t_i| > t_\alpha$ occurs show mutations exist in the sequence.

Cramer method

The difference between the Cramer method and the moving t-test is that t-test uses the mean difference of sub-sequence as the criterion, while the Cramer rule uses the mean difference of sub-sequence and total sequence as the criterion. If \bar{x} and \bar{x}_i are the mean values of the total sequence x and its sub-sequence x_i , and s is the variance of the total sequence, the statistics t are:

$$t = \sqrt{\frac{n_1(n-2)}{n-n_1(1+\tau^2)}} \tau \tag{7}$$

$$\tau = \frac{\bar{x}_i - \bar{x}}{s} \tag{8}$$

where n and n_1 represent the sequence length and the sub-sequence length. The sequence of statistics t_i ($i=1, 2, \dots, n-n_1+1$) can be obtained by sliding after determining n_1 . Similar to the moving t -test, if $|t_i| > t_\alpha$ occurs show mutations exist in the sequence.

Yamamoto method

Yamamoto method determines whether mutations exist by testing whether the difference between the sequence means is significant. The SNR is defined as follows:

$$SNR = \frac{|\bar{x}_1 - \bar{x}_2|}{s_1 + s_2} \tag{9}$$

In the formula, \bar{x}_1 and \bar{x}_2 are the mean values of the two sub-sequences x_1 and x_2 , and s_1 and s_2 are the standard deviations, respectively. Mutation and strong mutation exist when SNR is greater than 1 and 2, respectively.

Lepage method

The Lepage method is a two-sample nonparametric test whose statistics consist of the sum of standard Wilcoxon and Ansarity-Bradley tests. The n_1 and n_2 are assumed to be the variables of sub-sequence in the left and right of the

reference point, and the total sample size is n . The rank statistics are as follows:

$$W = \sum_{i=1}^n iU_i \tag{10}$$

In the formula, the U_i equals to 1 and 0 when the minimum value is before and after the reference point, respectively. The W is the cumulative number of two sub-sequences, its mean and variance are as follow:

$$E(W) = \frac{1}{2}n_1(n_1 + n_2 + 1) \tag{11}$$

$$V(W) = \frac{1}{12}n_1n_2(n_1 + n_2 + 1) \tag{12}$$

Herein construct another rank statistic is as follows:

$$A = \sum_{i=1}^{n_1} iU_i + \sum_{i=n_1+1}^n (n-i+1)U_i \tag{13}$$

When n is an even number, the mean and variance of A are as follow:

$$E(A) = \frac{1}{4}n_1(n_1 + n_2 + 2) \tag{14}$$

$$V(A) = \frac{n_1n_2(n_1 + n_2 - 2)(n_1 + n_2 + 2)}{48 \times (n_1 + n_2 - 1)} \tag{15}$$

When n is an odd number, the mean and variance values of A are as follow:

$$E(A) = \frac{n_1(n_1 + n_2 + 1)^2}{4(n_1 + n_2)} \tag{16}$$

$$V(A) = \frac{n_1n_2(n_1 + n_2 + 1)((n_1 + n_2)^2 + 3)}{48 \times (n_1 + n_2)^2} \tag{17}$$

At this point, the joint statistic HK can be constructed as follows:

$$HK = \frac{(W - E(W))^2}{V(W)} + \frac{(A - E(A))^2}{V(A)} \tag{18}$$

When HK_i exceeds the critical value, it indicates that there is a significant difference between the samples before and after time i and the mutation occurred.

Mann-Kendall test method

As a common nonparametric statistical test method, the Mann-Kendall test has the advantage that it does not require

the test samples to follow a specific distribution and is not disturbed by a few outliers. Suppose there is a climate series x_1, x_2, x_N, m_i represents the cumulative number of $x_i > j$ ($1 \leq j \leq i$) and defines the statistic:

$$d_k = \sum_{i=1}^k m_i \quad (19)$$

Under the assumption of time series is random and independence, the mean and variance of d_k are as follow:

$$E(d_k) = \frac{k(k-1)}{4} \quad (20)$$

$$var(d_k) = \frac{k(k-1)(2k+5)}{72} \quad (2 \leq k \leq N) \quad (21)$$

Standardize the d_k to the following:

$$u(d_k) = \frac{(d_k - E(d_k))}{\sqrt{var(d_k)}} \quad (22)$$

When $|u| > u_\alpha$, it shows that there is an obvious change trend in the sequence with the given significance level α . Reference this method to the inverse sequence to get $\bar{u}(d_i)$, if the intersection of $u(d_k)$ and $\bar{u}(d_i)$ curve is between the reliability lines, then it is the mutation point.

Acknowledgements The authors sincerely acknowledge the insightful comments and corrections of editors and reviewers. Meanwhile, the technical guidance of consultant Dr. Seyed Hamidreza Sadeghi is highly acknowledged.

Author contribution All authors contributed to the study conception and design. Qingxia Lin performed the data analysis and drafted the paper; Zhiyong Wu designed the study and improved the manuscript; Jingjing Liu committed to data acquisition; Vijay P. Singh improved the manuscript revision; Zheng Zuo edited the writing.

Funding This work was jointly supported by the National Natural Science Foundation of China (Grant number 52009065), the Natural Science Foundation of Hubei province, China (Grant number 2020CFB293), and the NSFC-MWR-CTGC Joint Yangtze River Water Science Research Project (Grant number U2240225).

Data availability The raw datasets used for model establishment are open source. The meteorological data are available on the Internet at <http://data.cma.cn/>. The global 10-km soil profile dataset and global 1-km land cover classification dataset can refer to Reynolds et al (2000) and Hansen et al (2000), respectively. However, the model output dataset cannot be shared at this time as the data also forms part of an ongoing study.

Declarations

Conflict of interest The authors declare no competing interests.

References

- Abdelkader M, Yerdelen C (2022) Hydrological drought variability and its teleconnections with climate indices. *J Hydrol* 605:127290. <https://doi.org/10.1016/j.jhydrol.2021.127290>
- Aghelpour P, Bahrami-Pichaghchi H, Varshavian V (2021) Hydrological drought forecasting using multi-scalar streamflow drought index, stochastic models and machine learning approaches, in northern Iran. *Stochastic Environ Res Risk Assess* 35(8):1615–1635. <https://doi.org/10.1007/s00477-020-01949-z>
- Ahmed K, Shahid S, Chung ES, Wang XJ, Harun SB (2019) Climate change uncertainties in seasonal drought severity-area-frequency curves: case of arid region of Pakistan. *J Hydrol* 570:473–485. <https://doi.org/10.1016/j.jhydrol.2019.01.019>
- Altn TB, Sar F, Altn BN (2020) Determination of drought intensity in Seyhan and Ceyhan River basins, Turkey, by hydrological drought analysis. *Theor Appl Climatol* 139(1–2):95–107. <https://doi.org/10.1007/s00704-019-02957-y>
- Boone AA, Habets F, Noilhan J, Clark D, Yang ZL (2004) The rhône-aggregation land surface scheme intercomparison project: an overview. *J Clim* 17(1):187–208. [https://doi.org/10.1175/1520-0442\(2004\)017%3c0187:TRLSSI%3e2.0.CO;2](https://doi.org/10.1175/1520-0442(2004)017%3c0187:TRLSSI%3e2.0.CO;2)
- Chatterjee S, Khan A, Akbari H, Wang Y (2016) Monotonic trends in spatio-temporal distribution and concentration of monsoon precipitation (1901–2002) West Bengal. *India. Atmos Res* 182(12):54–75. <https://doi.org/10.1016/j.atmosres.2016.07.010>
- Chen X, Li FW, Li JZ, Feng P (2019) Three-dimensional identification of hydrological drought and multivariate drought risk probability assessment in the Luanhe River basin, China. *Theor Appl Climatol* 137:3055–3076. <https://doi.org/10.1007/s00704-019-02780-5>
- Diaz V, Corzo G, Lanen HV, Solomatine DP, Varouchakis EA (2019) Characterization of the dynamics of past droughts. *Sci Total Environ* 718:134588. <https://doi.org/10.1016/j.scitotenv.2019.134588>
- Dikshit A, Pradhan B, Alamri AM (2021) Long lead time drought forecasting using lagged climate variables and a stacked long short-term memory model. *Sci Total Environ* 755(2):142638. <https://doi.org/10.1016/j.scitotenv.2020.142638>
- Ding YH, Li Y, Wang ZY, Si D, Liu YJ (2020) Interdecadal variation of Afro-Asian summer monsoon: coordinated effects of AMO and PDO oceanic modes. *Trans Atmos Sci* 43(1):20–32 (In Chinese) <https://d.wanfangdata.com.cn/periodical/njqxxyxb202001005>
- Ding YB, Xu JT, Wang XW, Cai HJ, Zhou ZQ, Sun YA, Shi YH (2021) Propagation of meteorological to hydrological drought for different climate regions in China. *J Environ Manage* 283:111980. <https://doi.org/10.1016/j.jenvman.2021.111980>
- Fischer T, Gemmer M, Su B, Scholten T (2013) Hydrological long-term dry and wet periods in the Xijiang River basin. *South China Hydrol Earth Syst Sci* 17(1):135–148. <https://doi.org/10.5194/hess-17-135-2013>
- Gu L, Chen J, Yin JB, Xu CY, Chen H (2020) Drought hazard transferability from meteorological to hydrological propagation. *J Hydro* 585:124761. <https://doi.org/10.1016/j.jhydrol.2020.124761>
- Han ZM, Huang SZ, Huang Q, Leng GY, Liu Y, Bai QJ, He PX, Liang H, Shi WZ (2021) Grace-based high-resolution propagation threshold from meteorological to groundwater drought. *Agric for Meteorol* 307:108476. <https://doi.org/10.1016/j.agrformet.2021.108476>
- Hansen MC, Defries RS, Townshend J, Sohlberg R (2000) Global land cover classification at 1 km spatial resolution using a classification tree approach. *Int J Remote Sens* 21(6–7):1331–1364. <https://doi.org/10.1080/014311600210209>
- Henriques A, Santos M (1999) Regional drought distribution model. *Phys Chem Earth Part B Hydrol. Oceans Atmos* 24:19–22. [https://doi.org/10.1016/S1464-1909\(98\)00005-7](https://doi.org/10.1016/S1464-1909(98)00005-7)

- Huang SZ, Huang Q, Chang JX, Leng GY (2016) Linkages between hydrological drought, climate indices and human activities: a case study in the Columbia River basin. *Int J Climatol* 36(1):280–290. <https://doi.org/10.1002/joc.4344>
- Huang SZ, Li P, Huang Q, Leng GY, Hou BB, Ma L (2017) The propagation from meteorological to hydrological drought and its potential influence factors. *J Hydro* 547:184–195. <https://doi.org/10.1016/j.jhydrol.2017.01.041>
- Huang Y, Wang H, Xiao WH, Chen LH, Yan DH, Zhou YY, Jiang DC, Yang MZ (2018) Spatial and temporal variability in the precipitation concentration in the upper reaches of the Hongshui River basin, southwestern China. *Adv Meteorol* 1:1–19. <https://doi.org/10.1155/2018/4329757>
- Kambombe O, Ngongondo C, Eneya L, Monjerezi M, Boyce C (2021) Spatio-temporal analysis of droughts in the Lake Chilwa Basin, Malawi. *Theor Appl Climatol* 144:1219–1231. <https://doi.org/10.1007/s00704-021-03586-0>
- Katipolu OM, Acar R, Senocak S (2021) Spatio-temporal analysis of meteorological and hydrological droughts in the Euphrates basin. *Turkey Water Sci Technol Water Supply* 21(4):1657–1673. <https://doi.org/10.2166/ws.2021.019>
- Kumar KS, Anandraj P, Sreelatha K, Sridhar V (2021) Regional analysis of drought severity-duration-frequency and severity-area-frequency curves in the Godavari River basin. *India Int J Climatol* 41(12):5481–5501. <https://doi.org/10.1002/joc.7137>
- Li SL, Bates GT (2007) Influence of the Atlantic multidecadal oscillation on the winter climate of east China. *Adv Atmos Sci* 24(1):126–135. <https://doi.org/10.1007/s00376-007-0126-6>
- Li Z, Su YX (2009) The analysis on precipitation variation characteristic in Guangxi from 1961 to 2004. *Chin Agric Sci Bull* 25(15):268–272 (In Chinese) <https://d.wanfangdata.com.cn/periodical/zgnxtb200915059>
- Li DP, Mu PF, Bai T, Huang Q, Huang SZ, Zhang Y (2020) Meteorological drought characteristics and driving force analysis of Xijiang River Basin based on variable scale SPI. *J Xi'an Univ Technol* 36(1):41–50 (In Chinese) <https://doi.org/10.19322/j.cnki.issn.1006-4710.2020.01.006>
- Li ZL, Quan XS, Tian QY, Zhang LY (2020b) Copula-based drought severity-area-frequency curve and its uncertainty, a case study of Heihe River basin. *China Hydrol Res* 51(2):867–881. <https://doi.org/10.2166/nh.2020.173>
- Li JY, Wu CH, Xia CA, Yeh PJF, Hu BX, Huang GR (2021) Assessing the responses of hydrological drought to meteorological drought in the Huai River Basin, China. *Theor Appl Climatol* 144:1043–1057. <https://doi.org/10.1007/s00704-021-03567-3>
- Li YL, He R, Qin WJ (2010) Influence of climate change on drought disaster in Guangxi. *Meteorol environ res.* 1(6):62–65 (In Chinese) <https://doi.org/10.3969/j.issn.0517-6611.2010.21.098>
- Liang X, Lettenmaier DP, Wood EF, Burges SJ (1994) A simple hydrologically based model of land surface water and energy fluxes for general circulation models. *J Geophys Res Atmos* 99(D7):14415–14428. <https://doi.org/10.1029/94JD00483>
- Lin QX, Wu ZY, Singh VP, Sadeghi S, He H, Lu GH (2017) Correlation between hydrological drought, climatic factors, reservoir operation, and vegetation cover in the Xijiang basin, South China. *J Hydrol* 549:512–524. <https://doi.org/10.1016/j.jhydrol.2017.04.020>
- Lin QX (2018) Analysis of Hydrological drought evolution and its interaction with environment factors in the Xijiang River basin. Dissertation, Hohai University (In Chinese)
- Liu Z, Huang Q, Yang YY, Huang SZ (2020) Diagnosis and driving force analysis of variations in precipitation-temperature relation of Xijiang River basin. *J Hydroelectric Eng* 39(10):57–71 (In Chinese) <https://doi.org/10.11660/slfdbx.20201004>
- Lu GH, Liu JJ, Wu ZY, He H, Xu HT, Lin QX (2015) Development of a large-scale routing model with scale independent by considering the damping effect of sub-basins. *Water Resour Manage* 29(14):5237–5253. <https://doi.org/10.1007/s11269-015-1115-7>
- Mahmoudi P, Rigi A, Kamak MM (2019) A comparative study of precipitation-based drought indices with the aim of selecting the best index for drought monitoring in Iran. *Theor Appl Climatol* 147:3123–3138. <https://doi.org/10.1007/s00704-019-02778-z>
- Margariti J, Rangelcroft S, Parry S, Wendt DE, Van Loon AF (2019) Anthropogenic activities alter drought termination. *Elem Sci Anth* 7:27. <https://doi.org/10.1525/elementa.365>
- Melsen LA, Guse B (2019) Hydrological drought simulations: how climate and model structure control parameter sensitivity. *Water Resour Res* 55(12):10527–10547. <https://doi.org/10.1029/2019WR025230>
- Meng CQ, Zhou JZ, Muhammad T, Shuang Z, Zhang HR (2016) Integrating artificial neural networks into the VIC model for rainfall-runoff modeling. *Water* 8(9):407. <https://doi.org/10.3390/w8090407>
- Mishra A, Desai V (2005) Spatial and temporal drought analysis in the Kansabati river basin. *India Int J River Basin Manag* 3:31–41. <https://doi.org/10.1080/15715124.2005.9635243>
- Mishra AK, Singh VP (2009) Analysis of drought severity–area–frequency curves using a general circulation model and pattern uncertainty. *J Geophys Res* 114:D06120. <https://doi.org/10.1029/2008JD010986>
- Monjo R, Royé D, Martin-Vide J (2020) Meteorological drought lacunarity around the world and its classification. *Earth Syst Sci Data* 12(1):741–752. <https://doi.org/10.5194/essd-12-741-2020>
- Nahler G (2009) Pearson Correlation Coefficient Springer Vienna. Chapter 1025:132–132. <https://doi.org/10.1007/978-3-211-89836-9>
- Nash JE, Sutcliffe JV (1970) River flow forecasting through conceptual models: part I-A discussion of principles. *J Hydrol* 10(3):282–290. [https://doi.org/10.1016/0022-1694\(70\)90255-6](https://doi.org/10.1016/0022-1694(70)90255-6)
- Niu J (2013) Precipitation in the Pearl River basin, South China: scaling, regional evolutions, and influence of large-scale climate anomalies. *Stochastic Environ Res Risk Assess* 27(5):1253–1268. <https://doi.org/10.1007/s00477-012-0661-2>
- Niu J, Chen J (2014) Terrestrial hydrological responses to precipitation variability in Southwest China with emphasis on drought. *Hydrol Sci J* 59(2):325–335. <https://doi.org/10.1080/02626667.2013.822641>
- Niu J, Chen J, Sun L (2015) Exploration of drought evolution using numerical simulations over the Xijiang (West River) basin in South China. *J Hydrol* 526:68–77. <https://doi.org/10.1016/j.jhydrol.2014.11.029>
- Noorisameleh Z, Gough WA, Mirza M (2021) Persistence and spatial-temporal variability of drought severity in Iran. *Environ Sci Pollut Res* 28:48808–48822. <https://doi.org/10.1007/s11356-021-14100-4>
- Qian CC, Yu JY, Chen G (2014) Decadal summer drought frequency in China: the increasing influence of the Atlantic Multi-decadal Oscillation. *Environ Res Lett* 9:124004. <https://doi.org/10.1088/1748-9326/9/12/124004>
- Rangelcroft S, Van Loon AF, Maureira H, Verbist K, Hannah DM (2019) An observation-based method to quantify the human influence on hydrological drought: upstream downstream comparison. *Hydrol Sci J* 64:276–287. <https://doi.org/10.1080/0262667.2019.1581365>
- Reynolds CA, Jackson TJ, Rawls WJ (2000) Estimating soil water-holding capacities by linking the Food and Agriculture Organization soil map of the world with global pedon databases and continuous pedotransfer functions. *Water Resour Res* 36(12):3653–3662. <https://doi.org/10.1029/2000WR900130>
- Rosenbrock HH (1960) An automatic method for finding the greatest or least value of a function. *Comput J* 3(3):175–184. <https://doi.org/10.1093/comjnl/3.3.175>

- Scheidegger JM, Jackson CR, Muddu S, Tomer SK, Filgueira R (2021) Integration of 2D lateral groundwater flow into the variable infiltration capacity (VIC) model and effects on simulated fluxes for different grid resolutions and aquifer diffusivities. *Water* 13(5):663. <https://doi.org/10.3390/w13050663>
- Shan CH, Yuan F, Sheng D, Zhou L, Liu YP (2016) A simulation of climate change features under pattern to A1B in West River basin by PRECIS. *China Rural Water Hydropower*. 84–87 (In Chinese) http://en.cnki.com.cn/Article_en/CJFDTOTAL-ZNSD201612018.htm
- Shukla S, Wood AW (2008) Use of a standardized runoff index for characterizing hydrologic drought. *Geophys Res Lett* 35(2):226–236. <https://doi.org/10.1029/2007GL032487>
- Talaei PH, Tabari H, Ardakani SS (2014) Hydrological drought in the west of Iran and possible association with large-scale atmospheric circulation patterns. *Hydrol Processes* 28(3):764–773. <https://doi.org/10.1002/hyp.9586>
- Touseef M, Chen LH, Yang KP, Chen YY (2020) Long-term rainfall trends and future projections over Xijiang River Basin, China. *Adv Meteorol* 2020:1–18. <https://doi.org/10.1155/2020/6852148>
- Vazifekhah S, Kahya E (2019) Hydrological and agricultural droughts assessment in a semi-arid basin: inspecting the teleconnections of climate indices on a catchment scale. *Agric Water Manage* 217:413–425. <https://doi.org/10.1016/j.agwat.2019.02.034>
- Veetil AV, Mishra AK (2020) Multiscale hydrological drought analysis: role of climate, catchment and morphological variables and associated thresholds. *J Hydrol* 582(4):124533. <https://doi.org/10.1016/j.jhydrol.2019.124533>
- Venegas-Cordero N, Birkel C, Giraldo-Osorio JD, Correa-Barahona A, Nauditt A (2021) Can hydrological drought be efficiently predicted by conceptual rainfall-runoff models with global data products? *J Nat Resour Dev* 11(2):1–18. <https://doi.org/10.5027/jnrd.v11i0.02>
- Wada Y, Van Beek LP, Wanders N, Bierkens MF (2013) Human water consumption intensifies hydrological drought worldwide. *Environ Res Lett* 8:034036. <https://doi.org/10.1088/1748-9326/8/3/034036>
- Wang YM, Li SL, Luo DH (2009) Seasonal response of Asian monsoonal climate to be the Atlantic Multidecadal Oscillation. *J Geophys Res* 114:D02112. <https://doi.org/10.1029/2008jd010929>
- Wu ZY, Lin QX, Lu GH, He H, Qu JJ (2015) Analysis of hydrological drought frequency for the Xijiang River Basin in South China using observed streamflow data. *Nat Hazards* 77(3):1655–1677. <https://doi.org/10.1007/s11069-015-1668-z>
- Wu JF, Chen XH, Yu ZX, Yao HX, Li W, Zhang DJ (2019a) Assessing the impact of human regulations on hydrological drought development and recovery based on a ‘simulated-observed’ comparison of the SWAT model. *J Hydrol* 577:123990. <https://doi.org/10.1016/j.jhydrol.2019.123990>
- Wu JF, Chen XW, Chang TJ (2019b) Correlations between hydrological drought and climate indices with respect to the impact of a large reservoir. *Theor Appl Climatol* 139(1):727–739. <https://doi.org/10.1007/s00704-019-02991-w>
- Wu ZY, Lin QX (2016) Analysis on spatial and temporal characteristics of hydrological drought in Xijiang River basin. *Water resour. Prot.* 32(1): 51–56 (In Chinese) <https://doi.org/10.3880/j.issn.1004-6933.2016.01.008>
- Wu ZY, Liu QT, Liu JJ, Xu ZG (2021) Construction and validation of 10 km grid routing model in China. *J China Hydrol* 41(3):75–81 (In Chinese) <https://doi.org/10.19797/j.cnki.1000-0852.20190369>
- Xing Z, Ma M, Su Z, Lv J, Song W (2020) A review of the adaptability of hydrological models for drought forecasting. *Proc IAHS* 383:261–266. <https://doi.org/10.5194/piahs-383-261-2020>
- Yamazaki D, Oki T, Kanae S (2009) Deriving a global river network map and its sub-grid topographic characteristics from a fine-resolution flow direction map. *Hydrol Earth Syst Sci* 13(11):2241–2251. <https://doi.org/10.5194/hess-13-2241-2009>
- Yuan X, Zhang M, Wang LY, Zhou T (2017) Understanding and seasonal forecasting of hydrological drought in the Anthropocene. *Hydrol Earth Syst Sci* 21:5477–5492. <https://doi.org/10.5194/hess-21-5477-2017>
- Yuan F, Zhang YQ, Liu Y, Ma MW, Zhang LM, Shi JY (2021) Drought assessment of Xijiang River basin based on standardized Palmer drought index. *Water Resour Prot* 37(1):46–52 (In Chinese) <https://doi.org/10.3880/j.issn.1004-6933.2021.01.007>
- Zhang F (2012) Research on distributed hydrological simulation and its application in Xijiang River basin. Dissertation, Donghua University (In Chinese) <http://www.doc88.com/p-9488184731625.html>
- Zhang JP (2014) Change law and forecasting of the runoff in the Zhangze Reservoir based on nonlinear method. Doctoral dissertation. Dissertation, Xi'an University of Technology (In Chinese) <https://doi.org/10.7666/d.D548827>
- Zhang D, Zhang Q, Qiu JM, Bai P, Kang L, Li XH (2018) Intensification of hydrological drought due to human activity in the middle reaches of the Yangtze River, China. *Sci Total Environ* 637–638:1432–1442. <https://doi.org/10.1016/j.scitotenv.2018.05.121>
- Zhang RR, Wu XP, Zhou XZ, Ren BY, Zeng JY, Wang QF (2021) Investigating the effect of improved drought events extraction method on spatiotemporal characteristics of drought. *Theor Appl Climatol* 147:395–408. <https://doi.org/10.1007/s00704-021-03838-z>
- Zhang LJ, Li J (2018) Spatiotemporal change of drought at various time scales indicated by SPEI and SPI in Xijiang River basin. *Plateau Meteorol* 37(2):560–567 (In Chinese) <https://doi.org/10.7522/j.issn.1000-0534.2018.00013>
- Zhu Y, Liu Y, Wang W, Singh VP, Ma XY, Yu ZG (2019) Three-dimensional characterization of meteorological and hydrological droughts and their probabilistic links. *J Hydrol* 578:124016. <https://doi.org/10.1016/j.jhydrol.2019.124016>
- Zhu LJ, Cooper DJ, Han SJ, Yang JW, Zhang YD, Li ZS, Zhao HY, Wang XC (2021) Influence of the Atlantic multidecadal oscillation on drought in northern Daxing'an mountains. *Northeast China Catena* 198:105017. <https://doi.org/10.1016/j.catena.2020.105017>

Publisher's note Springer Nature remains neutral with regard to jurisdictional claims in published maps and institutional affiliations.